Biomol NMR Assign (2007) 1:117–120
DOI 10.1007/s12104-007-9041-0

ARTICLE

# $^{13}C$ and $^{15}N$ chemical shift assignments and secondary structure of the B3 immunoglobulin-binding domain of streptococcal protein G by magic-angle spinning solid-state NMR spectroscopy

**Philippe S. Nadaud · Jonathan J. Helmus · Christopher P. Jaroniec**

Received: 6 June 2007 / Accepted: 29 June 2007 / Published online: 28 July 2007


**Abstract** Complete $^{13}C$ and $^{15}N$ assignments of the B3 IgG-binding domain of protein G (GB3) in the microcrystalline solid phase, obtained using 2D and 3D MAS NMR, are presented. The chemical shifts are used to predict the protein backbone conformation and compared with solution-state shifts.

**Keywords** Immunoglobulin-binding domain · Protein G · Magic-angle spinning · Solid-state NMR

## Biological context

Protein G is a multidomain protein found on the cell surface of group G *Streptococcus* (Boyle 1990; Gronenborn et al. 1991). It binds to immunoglobulin G (IgG) with high affinity, and is believed to aid the bacterium in overcoming the immune response of the host. The binding to IgG is mediated by three homologous domains of ~55 aa, named B1, B2 and B3, which retain their IgG-binding properties when expressed individually (Boyle 1990) and have been utilized for a variety of biomedical applications (e.g., antibody purification). Moreover, since the initial structural characterization of the B1 domain by solution-state NMR (Gronenborn et al. 1991), the B domains of protein G (i.e., GB1, GB2, and GB3) have gained popularity as highly-versatile model systems for fundamental studies of protein stability, folding, structure, and dynamics (Gronenborn et al. 1991; Alexander et al. 1992; Derrick and Wigley 1994; Ulmer et al. 2003; Hall and Fushman 2003; Clore and Schwieters 2004; Franks et al. 2005).

The 3D structures of several B domains of protein G have been determined to very high resolution using solution-state NMR and X-ray crystallography as discussed thoroughly in (Gronenborn et al. 1991; Derrick and Wigley 1994; Ulmer et al. 2003) and references cited therein, and recently also by magic-angle spinning (MAS) solid-state NMR (C. M. Rienstra, personal communication). Despite some minor differences, all B domains characterized so far exhibit a similar, highly-compact fold consisting of a four-stranded $\beta$-sheet (with the central $\beta$1 and $\beta$4 strands in a parallel arrangement, and the outer $\beta$2 and $\beta$3 strands antiparallel to $\beta$1 and $\beta$4, respectively), packed against a central $\alpha$-helix connecting strands $\beta$2 and $\beta$3. The highest resolution X-ray structure to date (refined to 1.1-Å) corresponds to GB3 (PDB ID: 1igd) (Derrick and Wigley 1994), and a homologous 56 aa construct, encompassing the most structured region of 1igd (see below), was subsequently used by Bax and co-workers (Ulmer et al. 2003) to measure an extensive set of residual dipolar coupling and hydrogen bond restraints, leading to a further refinement of the 1.1-Å X-ray structure (PDB ID: 2oed). The atomic resolution structure of this 56 aa GB3 domain (subsequently referred to simply as GB3), which differs from 1igd by two substitutions (T1M, T2Q) and the deletion of a 5 aa N-terminal fragment (Fig. 1A) and from 2gb1 (Gronenborn et al. 1991) by seven substitutions (T2Q, I6V, L7I, E19K, A24E, V29A, E42V), is one of the highest resolution 3D protein structures currently available (in particular with respect to the $H^N$ and $H^\alpha$ coordinates). This

**Electronic supplementary material** The online version of this article (doi:10.1007/s12104-007-9041-0) contains supplementary material, which is available to authorized users.

P. S. Nadaud · J. J. Helmus · C. P. Jaroniec (✉)
Department of Chemistry, The Ohio State University, 1035 Evans Laboratory, 100 West 18th Avenue, Columbus, OH 43210, USA
e-mail: jaroniec@chemistry.ohio-state.edu

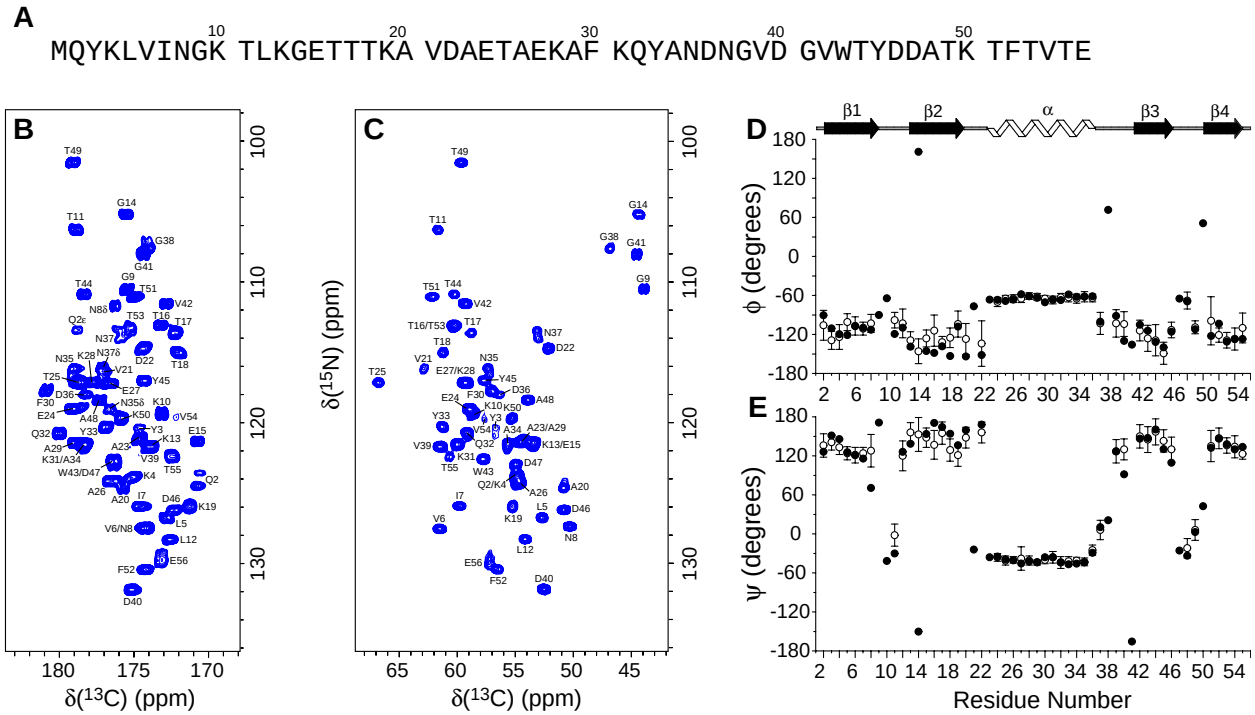


**Fig. 1** (**A**) Amino acid sequence of GB3. (**B**, **C**) Two-dimensional 500 MHz $N_i$-$C'_{i-1}$ (NCO; **B**) and $N_i$-$C_i^{\alpha}$ (NCA; **C**) correlation spectra (Hughes and Baldus 2005) of GB3 recorded at 11.111 kHz MAS rate. Spectra were recorded as 334* ($t_1$, $^{15}$N) × 1500* ($t_2$,$^{13}$C) data matrices with acquisition times of 30 ms ($t_1$) and 30 ms ($t_2$), and a measurement time of 7.5 h per spectrum. Spectra were processed using sine-bell window functions shifted by 60° in $F_1$ and $F_2$ (see Supporting Information Fig. S1 for additional experimental parameters). Cross-peaks are drawn with the lowest contour at ca. 40 times the rms noise level and labeled with the residue number according to the $^{15}$N frequency. (**D**, **E**) Analysis of backbone torsion angles in microcrystalline GB3 using the TALOS program (Cornilescu et al. 1999). Solid and open circles correspond to the $\varphi$ and $\psi$ torsion angle values found in the 2oed structure (Ulmer et al. 2003) and predicted using TALOS, respectively. The TALOS predictions include the reported estimated standard deviations and only the predictions where the program converged (46 out of 54 residues) are shown

has led to the extensive use of GB3 as a model system for the detailed analysis of protein structure, conformational dynamics and correlated backbone motions (Ulmer et al. 2003; Hall and Fushman 2003; Clore and Schwieters 2004).

Here, we present the complete backbone and side-chain $^{13}$C and $^{15}$N chemical shift assignments of GB3 in the microcrystalline solid phase, obtained using 2D and 3D MAS solid-state NMR (SSNMR) techniques. The chemical shifts for GB3 are used to predict the protein backbone conformation in the solid state, and compared with the corresponding solution-state shifts. This study complements the complete SSNMR backbone and side-chain $^{13}$C and $^{15}$N assignments reported recently for the T2Q mutant of GB1 by Rienstra and co-workers (Franks et al. 2005), as well as for several other microcrystalline proteins (Pauli et al. 2001; Bockmann et al. 2003; Igumenova et al. 2004; McDermott 2004; Hughes and Baldus 2005), and establishes GB3 as a valuable model system for the development of novel SSNMR methodology and for the fundamental atomic-level studies of protein structure, dynamics and intermolecular interactions in the solid phase.

## Methods and experiments

The plasmid encoding GB3 was kindly provided by Dr. Ad Bax (National Institutes of Health), and $^{13}$C,$^{15}$N-labeled GB3 was prepared using standard methods (Ulmer et al. 2003; Franks et al. 2005). Briefly, *E. coli* BL21(DE3) cells, transformed with the GB3 plasmid, were grown at 37°C using a minimal medium containing 1 g/l $^{15}NH_4Cl$, 2 g/l U-$^{13}$C-glucose and 10 ml of 10× BioExpress $^{13}$C,$^{15}$N-labeled rich-medium supplement (Cambridge Isotope Laboratories). Protein expression was induced at an $OD_{600}$ of ~0.7, using 0.5 mM isopropyl ß-D-thiogalactoside at 37°C for 4 h. GB3 was purified by heating the cell pellet, resuspended in 40 ml of phosphate buffered saline (1.7 mM $KH_2PO_4$, 5 mM $Na_2HPO_4$, 150 mM NaCl, pH 7.4), at 80°C for 5 min, followed by the concentration of the supernatant using Amicon Ultra-15 5,000 MWCO

devices (Millipore) and gel filtration chromatography using a HiLoad 16/60 Superdex 75 prep grade column (Amersham Biosciences/GE Healthcare) equilibrated with a 50 mM sodium phosphate, 150 mM NaCl, pH 6.5 buffer. Peak fractions containing the protein were collected, the buffer thoroughly exchanged to 50 mM sodium phosphate, pH 6.5, containing 0.02% (w/v) sodium azide, and the solution concentrated to ~30 mg/ml protein using Amicon Ultra-15 5,000 MWCO devices. This procedure typically yielded ~60–80 mg of purified protein per 1 l of culture.

Reference solution-state NMR spectra ($^{1}$H-$^{15}$N HSQC, 3D HNCO, HNCA, HN(CO)CA and HN(CA)CB), used to obtain the $^{1}H^{N}$, $^{15}$N, $^{13}C'$, $^{13}C^{\alpha}$ and $^{13}C^{\beta}$ chemical shifts, were recorded at 25 °C using a 600 MHz Bruker spectrometer equipped with a triple resonance pulsed field gradient probe, and ~1.5 mM GB3 in an aqueous sodium phosphate buffer, 50 mM, pH 6.5, 7% $D_2O$, and 0.02% (w/v) sodium azide. For SSNMR measurements, GB3 microcrystals were prepared by microdialysis at 4°C (starting with the ~30 mg/ml GB3 solution in 50 mM sodium phosphate, pH 6.5 buffer) using Hampton Research microdialysis buttons and a precipitant solution containing 2-methylpentane-2,4-diol, isopropanol, and deionized water in a 2:1:1 (v/v) ratio. Crystallization was allowed to proceed for at least 48 h, and the microcrystals (~20 mg; 3 μmol protein) were center-packed in a thin-wall 3.2 mm Varian rotor by centrifugation. SSNMR spectra were acquired using a 500 MHz three-channel Varian spectrometer equipped with a Varian 3.2 mm BioMAS HXY probe, at 11.111 kHz ± 3 Hz MAS rate and an effective sample temperature of 5°C. The following 2D and 3D chemical shift correlation experiments (McDermott 2004; Hughes and Baldus 2005) were used to establish the sequential assignments: 2D $^{13}$C–$^{13}$C (CC; $\tau_{mix,CC}$ = 5 and 25 ms), 2D $^{15}$N–$^{13}C^{\alpha}$ (NCA), 2D $^{15}$N–$^{13}C'$ (NCO), 2D $^{15}$N–($^{13}C^{\alpha}$)–$^{13}$CX (N(CA)CX; $\tau_{mix,CC}$ = 15 and 50 ms), 2D $^{15}$N–($^{13}C'$)–$^{13}$CX (N(CO)CX; $\tau_{mix,CC}$ = 15 and 50 ms), 3D $^{13}C'$–$^{15}$N–$^{13}C^{\alpha}$ (CONCA), 3D $^{15}$N–$^{13}C^{\alpha}$–$^{13}$CX (NCACX; $\tau_{mix,CC}$ = 50 ms), and 3D $^{15}$N–$^{13}C'$–$^{13}$CX (NCOCX; $\tau_{mix,CC}$ = 50 ms). Note that in all experiments homonuclear $^{13}$C–$^{13}$C magnetization transfer was accomplished using proton-driven spin diffusion, enhanced by the simultaneous application of a $n$ = 1 rotary resonant field on $^{1}$H (i.e., rf assisted spin diffusion (RAD)/dipolar assisted rotational resonance (DARR) mixing scheme) (Takegoshi et al. 2001; Morcombe et al. 2004), $^{15}$N-$^{13}C^{\alpha}$/$^{13}C'$ correlations were established using SPECIFIC cross-polarization (Baldus et al. 1998), and two pulse phase modulated (TPPM) $^{1}$H decoupling (Bennett et al. 1995) was applied during all chemical shift evolution periods. Additional details of the acquisition and processing parameters can be found in the Supporting Information. Chemical shifts in solution and solid phase were referenced using the DSS scale.

## Assignments and data deposition

Complete backbone and side-chain $^{13}$C and $^{15}$N chemical shift assignments of microcrystalline GB3 are presented in Table S1. Representative 2D NCA and NCO spectra, showing the quality of the NMR data, are shown in Fig. 1B,C (see Fig. S1 for additional details), and regions from 2D CC, N(CA)CX, N(CO)CX and 3D NCACX, NCOCX and CONCA spectra are shown in Figs. S2–S4. The chemical shifts have been deposited in the BioMagResBank (http://www.bmrb.wisc.edu) under the accession number 15283.

The 2D and 3D spectra enabled the detection of all the backbone and side-chain $^{13}$C and $^{15}$N resonances for GB3, in analogy to the recent study of microcrystalline GB1 (Franks et al. 2005). While the structural disorder (which would lead to increased inhomogeneous linebroadening) appears to be relatively minor overall for the protein microcrystals used here, as evidenced by a number of well-resolved $^{13}C'$–$^{13}C^{\alpha}$ J-couplings observed in the spectra in Fig. 1, we note that sets of signals originating from residues near the loops and termini (e.g., Q2, Y3, A20, V21, N37, N38, V54, T55, E56) do exhibit increased linebroadening particularly in the $^{15}$N dimension (and in several cases peak doubling in spectra recorded with the highest digital resolution), relative to signals from residues in regular secondary structure elements. In addition, $^{13}$C signals corresponding to aromatic side-chains (especially Phe and Tyr) were typically quite broad (~1–2 ppm) as observed also for microcrystalline GB1 (Franks et al. 2005), and certain side-chain resonances (e.g., I7$\delta$) exhibited significantly reduced intensities, most likely due to the attenuation of $^{1}$H–$^{13}$C and/or $^{13}$C–$^{13}$C dipolar couplings resulting from side-chain conformational exchange.

To assess the secondary structure and overall fold of GB3 in the microcrystalline solid phase, the isotropic $^{13}$C and $^{15}$N chemical shifts were used to predict the backbone $\varphi$ and $\psi$ dihedral angles within the program TALOS (Cornilescu et al. 1999). The comparison of TALOS-predicted torsion angles and the values found in the 2oed structure (Ulmer et al. 2003) is shown in Fig. 1D,E, and indicates that the protein secondary structure (and hence likely the overall fold) obtained using X-ray crystallography and solution-state NMR persists also in the microcrystalline phase. In summary, TALOS was considered to have converged (defined here as 8 or more self-consistent hits in a particular region of the Ramachandran map) for 46 out of 54 possible residues (with G9, K10, V21, A23, G38, G41, D47, K50: <8 consistent hits (excluded from analysis); T11, W43: 8 hits; L12, A26, D40, T51: 9 hits; remaining 40 residues: 10 hits). For the residues where TALOS converged, 35 $\varphi$ predictions were within ±1$\sigma$ of the corresponding $\varphi$ value in 2oed, 10 were within ±2$\sigma$,

and only one prediction (G14) deviated by more than $2\sigma$. For $\psi$, 36 predictions were within $\pm 1\sigma$, 7 were within $\pm 2\sigma$, and 3 (N8, G14, D40) differed by more than $2\sigma$. As also pointed out by others (Franks et al. 2005), we find that virtually all the non-convergent or incorrect TALOS predictions for GB3 correspond to glycines, residues directly adjacent to a glycine in the protein sequence, and residues found in the loops.

The backbone $^{13}C$ and $^{15}N$ chemical shifts in GB3 microcrystals were also compared to the corresponding shifts in solution (Fig. S5). Although several shifts (e.g., V42 and W43 $^{15}N$) show significant (>5 ppm) differences between solution and solid phases, the overall agreement is reasonable, with the mean shift differences ($\delta_{solid} - \delta_{solution}$) of $-0.3 \pm 0.9$ ppm for $^{13}C'/^{13}C^{\alpha}/^{13}C^{\beta}$ and $-1.3 \pm 2.4$ for amide $^{15}N$. These magnitudes of backbone $^{13}C$ and $^{15}N$ chemical shift deviations are on the order of those observed for other microcrystalline proteins (Bockmann et al. 2003; Igumenova et al. 2004; Franks et al. 2005; Balayssac et al. 2007), which indicates no major structural perturbations for GB3 in the microcrystalline phase relative to the protein in solution and supports the conclusions based on the TALOS analysis. Finally, we compared the $^{13}C'$, $^{13}C^{\alpha}$, $^{13}C^{\beta}$ and backbone $^{15}N$ chemical shifts for the conserved residues (total of 200 chemical shifts for 50 residues) in microcrystalline GB3 with those reported by (Franks et al. 2005) in their GB1 study (Fig. S6). Overall, the chemical shifts for these two homologous proteins are as highly correlated as could be expected, which indicates that, as in single crystals ($C^{\alpha}$ RMSD of 0.33 Å for 1pgb and 2oed structures), GB1 and GB3 also adopt very similar three-dimensional structures in the microcrystalline phase.

**Acknowledgments** This research was supported by the Ohio State University. The authors thank Dr. Ad Bax (National Institutes of Health) for the gift of the GB3 plasmid and Prof. Chad M. Rienstra (University of Illinois, Urbana-Champaign) for a control sample of $^{13}C$,$^{15}N$-labeled GB1, sharing unpublished data for GB3 crystallized using the batch method, and stimulating discussions related to sample preparation, and experimental protocols.

## References

Alexander P, Fahnestock S, Lee T, Orban J, Bryan P (1992) Thermodynamic analysis of the folding of the streptococcal protein G IgG-binding domains B1 and B2: why small proteins tend to have high denaturation temperatures. Biochemistry 31:3597–3603

Balayssac S, Bertini I, Falber K, Fragai M, Jehle S, Lelli M, Luchinat C, Oschkinat H, Yeo KJ (2007) Solid-state NMR of matrix metalloproteinase 12: an approach complementary to solution NMR. Chem Biochem 8:486–489

Baldus M, Petkova AT, Herzfeld J, Griffin RG (1998) Cross polarization in the tilted frame: assignment and spectral simplification in heteronuclear spin systems. Mol Phys 95:1197–1207

Bennett AE, Rienstra CM, Auger M, Lakshmi KV, Griffin RG (1995) Heteronuclear decoupling in rotating solids. J Chem Phys 103:6951–6957

Bockmann A, Lange A, Galinier A, Luca S, Giraud N, Juy M, Heise H, Montserret R, Penin F, Baldus M (2003) Solid state NMR sequential resonance assignments and conformational analysis of the $2 \times 10.4$ kDa dimeric form of the Bacillus subtilis. J Biomol NMR 27:323–339

Boyle MDP (1990) Bacterial immunoglobulin binding proteins. Academic Press, New York, NY, USA

Clore GM, Schwieters CD (2004) Amplitudes of protein backbone dynamics and correlated motions in a small $\alpha/\beta$ protein: correspondence of dipolar coupling and heteronuclear relaxation measurements. Biochemistry 43:10678–10691

Cornilescu G, Delaglio F, Bax A (1999) Protein backbone angle restraints from searching a database for chemical shift and sequence homology. J Biomol NMR 13:289–302

Derrick JP, Wigley DB (1994) The third IgG-binding domain from streptococcal protein G: An analysis by X-ray crystallography of the structure alone and in a complex with Fab. J Mol Biol 243:906–918

Franks WT, Zhou DH, Wylie BJ, Money BG, Graesser DT, Frericks HL, Sahota G, Rienstra CM (2005) Magic-angle spinning solid-state NMR spectroscopy of the $\beta 1$ immunoglobulin binding domain of protein G (GB1): $^{15}N$ and $^{13}C$ chemical shift assignments and conformational analysis. J Am Chem Soc 127:12291–12305

Gronenborn AM, Filpula DR, Essig NZ, Achari A, Whitlow M, Wingfield PT, Clore GM (1991) A novel, highly stable form of the immunoglobulin binding domain of streptococcal protein G. Science 253:657–661

Hall JB, Fushman D (2003) Characterization of the overall and local dynamics of a protein with intermediate rotational anisotropy: differentiating between conformational exchange and anisotropic diffusion in the B3 domain of protein G. J Biomol NMR 27:261–275

Hughes CE, Baldus M (2005) Magic-angle spinning solid-state NMR applied to polypeptides and proteins. Annu Rep NMR Spect 55:121–158

Igumenova TI, Wand AJ, McDermott AE (2004) Assignment of the backbone resonances for microcrystalline ubiquitin. J Am Chem Soc 126:5323–5331

McDermott AE (2004) Structural and dynamic studies of proteins by solid-state NMR spectroscopy: rapid movement forward. Curr Opin Struct Biol 14:554–561

Morcombe CR, Gaponenko V, Byrd RA, Zilm KW (2004) Diluting abundant spins by isotope edited radio frequency field assisted diffusion. J Am Chem Soc 126:7196–7197

Pauli J, Baldus M, van Rossum B, de Groot H, Oschkinat H (2001) Backbone and side-chain $^{13}C$ and $^{15}N$ signal assignments of the $\alpha$-spectrin SH3 domain by magic angle spinning solid-state NMR at 17.6 Tesla. Chem Biochem 2:272–281

Takegoshi K, Nakamura S, Terao T (2001) $^{13}C$–$^{1}H$ dipolar-assisted rotational resonance in magic-angle spinning NMR. Chem Phys Lett 344:631–637

Ulmer TS, Ramirez BE, Delaglio F, Bax A (2003) Evaluation of backbone proton positions and dynamics in a small protein by liquid crystal NMR spectroscopy. J Am Chem Soc 125:9179–9191

# Supporting Information

## $^{13}C$ and $^{15}N$ Chemical Shift Assignments and Secondary Structure of the B3 Immunoglobulin-Binding Domain of Streptococcal Protein G by Magic-Angle Spinning Solid-State NMR Spectroscopy

Philippe S. Nadaud, Jonathan J. Helmus, and Christopher P. Jaroniec*

*Department of Chemistry, The Ohio State University, Columbus, Ohio 43210*

Email: jaroniec@chemistry.ohio-state.edu

**Table S1.** $^{15}$N and $^{13}$C chemical shifts of microcrystalline GB3.[a]

| Residue | N | C′ | Cα | Cβ | Cγ | Cδ | Cε | Cζ | Cη | Nδ | Nε | Nζ |
|---|---|---|---|---|---|---|---|---|---|---|---|---|
| M1 | 39.0 | 170.7 | 54.9 | 33.5 | 30.4 | | 15.9 | | | | | |
| Q2 | 124.3 | 174.9 | 54.7 | 31.2 | 34.5 | 178.9 | | | | | 113.4 | |
| Y3 | 120.4 | 174.9 | 56.7 | 43.2 | 129.7 | 133.3 | 118.4 | 158.0 | | | | |
| K4 | 123.9 | 172.9 | 54.9 | 35.8 | 25.5 | 28.7 | 42.0 | | | | | 32.7 |
| L5 | 126.8 | 174.2 | 52.7 | 42.5 | 26.7 | 25.2 | | | | | | |
| | | | | | | 24.8 | | | | | | |
| V6 | 127.5 | 174.6 | 61.5 | 32.3 | 21.2 | | | | | | | |
| | | | | | 20.8 | | | | | | | |
| I7 | 125.9 | 174.3 | 59.8 | 40.4 | 28.2 | 15.4 | | | | | | |
| | | | | | 18.5 | | | | | | | |
| N8 | 127.3 | 175.6 | 50.3 | 38.3 | 176.4 | | | | | 111.8 | | |
| G9 | 110.5 | 173.2 | 43.8 | | | | | | | | | |
| K10 | 119.4 | 178.9 | 58.7 | 32.1 | 24.9 | 28.5 | 43.8 | | | | | 32.8 |
| T11 | 106.3 | 172.7 | 61.6 | 69.1 | 21.6 | | | | | | | |
| L12 | 128.3 | 174.0 | 54.1 | 42.2 | 27.9 | 24.9 | | | | | | |
| | | | | | | 24.0 | | | | | | |
| K13 | 121.6 | 175.6 | 53.6 | 39.0 | 26.7 | 30.2 | 42.6 | | | | | 30.7 |
| G14 | 105.2 | 170.8 | 44.3 | | | | | | | | | |
| E15 | 121.3 | 173.3 | 53.4 | 35.0 | 36.4 | 182.6 | | | | | | |
| T16 | 113.1 | 172.3 | 60.1 | 69.6 | 19.3 | | | | | | | |
| T17 | 113.6 | 172.1 | 58.7 | 71.6 | 20.2 | | | | | | | |
| T18 | 115.0 | 171.3 | 61.2 | 70.0 | 18.5 | | | | | | | |
| K19 | 125.9 | 175.8 | 55.2 | 33.5 | 25.6 | 29.3 | 41.9 | | | | | 33.0 |
| A20 | 124.5 | 177.2 | 50.8 | 23.1 | | | | | | | | |
| V21 | 116.2 | 174.4 | 62.9 | 32.0 | 23.2 | | | | | | | |
| | | | | | 21.4 | | | | | | | |
| D22 | 114.7 | 174.6 | 52.1 | 42.2 | 179.3 | | | | | | | |
| A23 | 121.2 | 179.2 | 54.3 | 17.8 | | | | | | | | |
| E24 | 119.0 | 178.6 | 58.9 | 28.8 | 36.1 | 182.8 | | | | | | |
| T25 | 117.1 | 176.6 | 66.8 | 67.7 | 21.8 | | | | | | | |
| A26 | 124.1 | 176.7 | 54.5 | 17.2 | | | | | | | | |
| E27 | 117.1 | 177.7 | 59.2 | 28.8 | 35.6 | 181.1 | | | | | | |
| K28 | 117.1 | 178.9 | 59.3 | 32.1 | 25.3 | 29.0 | 41.9 | | | | | 32.5 |
| A29 | 121.4 | 180.9 | 54.5 | 17.7 | | | | | | | | |
| F30 | 117.7 | 178.4 | 57.0 | 37.2 | 137.7 | 130.4 | 130.2 | | | | | |
| K31 | 121.5 | 180.0 | 60.0 | 31.7 | 26.5 | 29.1 | 40.8 | | | | | 31.9 |
| Q32 | 120.8 | 176.9 | 59.1 | 27.9 | 33.6 | 180.0 | | | | | 112.2 | |
| Y33 | 120.3 | 178.4 | 61.2 | 37.1 | 130.1 | 132.7 | 118.7 | 158.4 | | | | |
| A34 | 121.6 | 178.9 | 55.6 | 17.7 | | | | | | | | |
| N35 | 116.3 | 178.3 | 57.2 | 39.9 | 176.5 | | | | | 119.1 | | |
| D36 | 118.1 | 175.9 | 56.3 | 39.1 | 177.3 | | | | | | | |
| N37 | 113.7 | 174.2 | 53.1 | 40.0 | 177.0 | | | | | 116.6 | | |
| G38 | 107.5 | 173.9 | 46.8 | | | | | | | | | |
| V39 | 121.7 | 175.1 | 61.5 | 31.8 | 22.0 | | | | | | | |
| | | | | | 21.1 | | | | | | | |
| D40 | 131.8 | 174.4 | 52.5 | 41.1 | 180.3 | | | | | | | |
| G41 | 108.0 | 172.9 | 44.5 | | | | | | | | | |
| V42 | 111.5 | 176.4 | 59.3 | 33.2 | 22.4 | | | | | | | |
| | | | | | 18.8 | | | | | | | |
| W43 | 122.6 | 178.4 | 57.7 | 33.9 | 112.0 | 126.1 | 138.5 | 114.5 | 122.8 | | 130.9 | |
| | | | | | | 129.9 | 119.2 | 120.5 | | | | |
| T44 | 110.9 | 174.3 | 60.3 | 72.7 | 20.8 | | | | | | | |
| Y45 | 117.0 | 172.4 | 57.7 | 41.9 | 128.4 | 132.2 | 117.3 | 157.3 | | | | |
| D46 | 126.3 | 176.4 | 50.8 | 42.4 | 179.6 | | | | | | | |
| D47 | 123.0 | 177.4 | 54.9 | 42.7 | 179.0 | | | | | | | |
| A48 | 118.4 | 179.1 | 53.8 | 18.8 | | | | | | | | |
| T49 | 101.5 | 175.9 | 59.6 | 69.8 | 21.2 | | | | | | | |
| K50 | 119.7 | 175.1 | 55.3 | 27.2 | 24.7 | 27.5 | 43.4 | | | | | 32.8 |
| T51 | 111.0 | 174.3 | 62.1 | 71.8 | 21.0 | | | | | | | |
| F52 | 130.4 | 175.3 | 56.6 | 42.7 | 139.8 | 131.9 | 130.4 | | | | | |
| T53 | 113.3 | 172.3 | 60.4 | 71.5 | 19.9 | | | | | | | |
| V54 | 119.6 | 172.5 | 57.7 | 32.2 | 21.5 | | | | | | | |
| | | | | | 19.7 | | | | | | | |
| T55 | 122.4 | 173.2 | 60.7 | 71.5 | 22.0 | | | | | | | |
| E56 | 129.7 | 179.9 | 57.2 | 33.2 | 38.4 | 182.7 | | | | | | |

[a] Note that the assignment summary table above is provided for reference purposes only; the verified chemical shift assignments, consistent with the IUPAC nomenclature, have been deposited in the BioMagResBank (http://www.bmrb.wisc.edu) under the accession number 15283. Chemical shifts were referenced relative to DSS according to Morcombe and Zilm (Marcombe & Zilm, 2003), with adamantane used as a secondary standard and assuming the $^{13}$C chemical shift of 40.48 ppm for the downfield resonance. For resonances corresponding to well-structured regions of the protein the estimated uncertainty of most chemical shifts is ±0.1 ppm based upon variations observed in multiple data sets. Note, however, that in the GB3 sample used here, sets of signals originating from residues near the loops and termini (e.g., Q2, Y3, A20, V21, N37, N38, V54, T55, E56) exhibited increased linebroadening (and in a few cases peak doubling in spectra recorded with high digital resolution), particularly in the $^{15}$N dimension, relative to signals from residues in regular secondary structure elements. Note also, that $^{13}$C signals corresponding to aromatic side-chains (Phe and Tyr in particular) were typically quite broad (~1-2 ppm) and asymmetric, as observed in previous studies (Franks et al., 2005), resulting in a larger uncertainty of these chemical shifts.

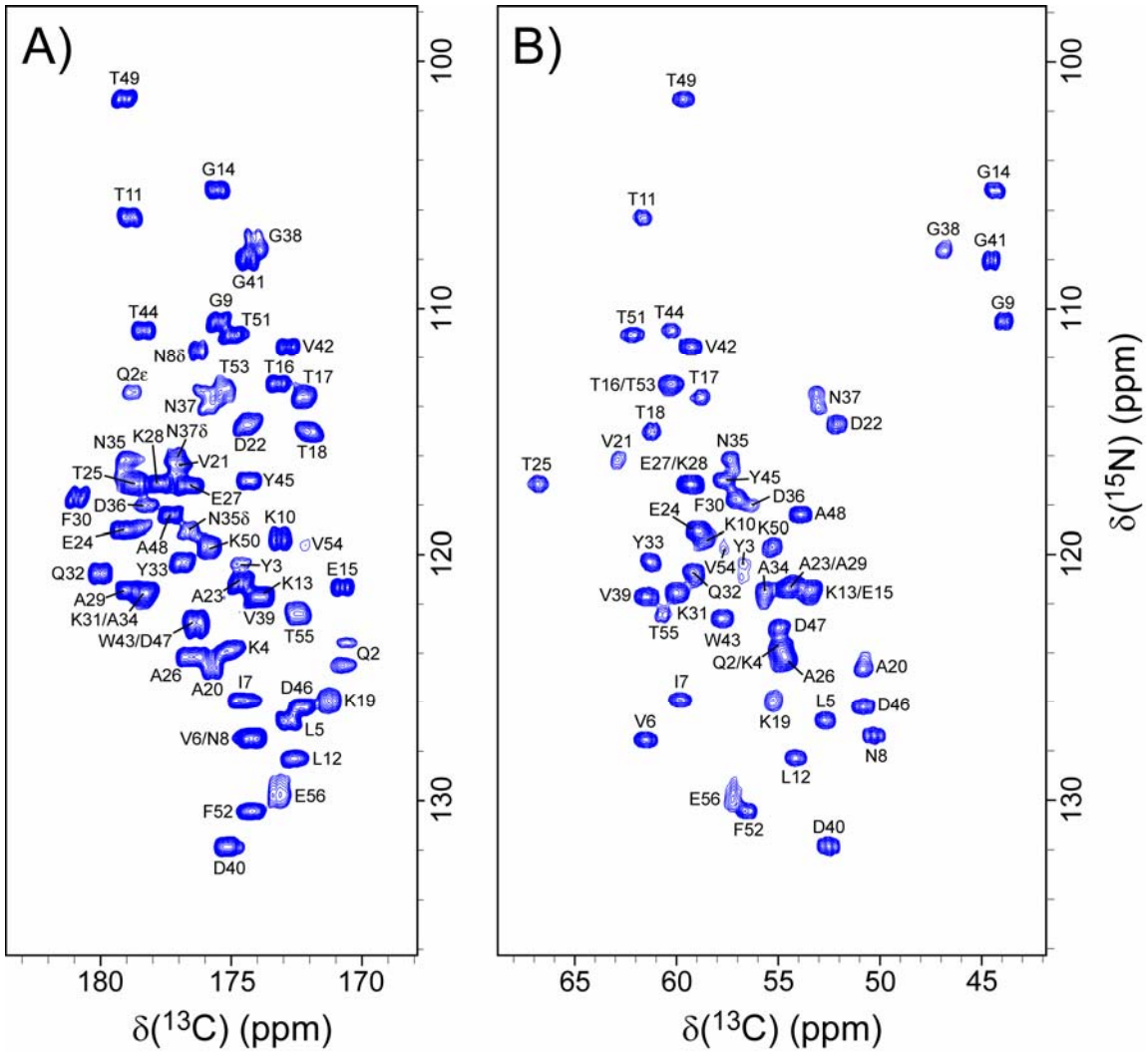


**Figure S1.** Two-dimensional 500 MHz $N_i$-$C'_{i-1}$ (NCO; A) and $N_i$-$C^{\alpha}_i$ (NCA; B) correlation spectra of GB3 recorded at 11.111 kHz MAS rate. Spectra were recorded as 334* ($t_1$, $^{15}$N) × 1500* ($t_2$,$^{13}$C) data matrices with acquisition times of 30 ms ($t_1$) and 30 ms ($t_2$), and a measurement time of 7.5 h per spectrum. Experimental parameters, NCO: $^{15}$N carrier at 120 ppm, $^{13}$C carrier at 177 ppm, 6 ms SPECIFIC cross-polarization (CP) (Baldus et al., 1998) with rf fields of ~7/2×$\omega_r$ on $^{15}$N and ~5/2×$\omega_r$ on $^{13}$C (with tangent ramp (Hediger et al., 1995)); NCA: $^{15}$N carrier at 120 ppm, $^{13}$C carrier at 90 ppm, 3.5 ms SPECIFIC CP with rf fields of ~7/2×$\omega_r$ on $^{15}$N and ~5/2×$\omega_r$ on $^{13}$C (with tangent ramp); common parameters: 1 ms $^{1}$H-$^{15}$N CP (50 kHz $^{1}$H, ~40 kHz $^{15}$N with tangent ramp), 70 kHz two-pulse phase modulated (TPPM) $^{1}$H decoupling (Bennett et al., 1995) during $t_1$ and $t_2$, single $^{13}$C π-pulse centered in $t_1$ for $^{15}$N-$^{13}C^{\alpha}$/$^{13}C'$ J-decoupling, rotor-synchronized $^{15}$N π-pulse train in $t_2$ for $^{15}$N-$^{13}$C J-decoupling (~28 kHz rf field, *xy*-8 phase cycling (Gullion et al., 1990), one pulse every 8 rotor cycles). Cross-peaks are drawn with the lowest contour at ca. 40 times the rms noise level and labeled with the residue number according to the $^{15}$N frequency. All spectra were processed in NMRPipe (Delaglio et al., 1995), typically using sine-bell window functions shifted by 60°, and analyzed using Sparky (Goddard & Kneller).

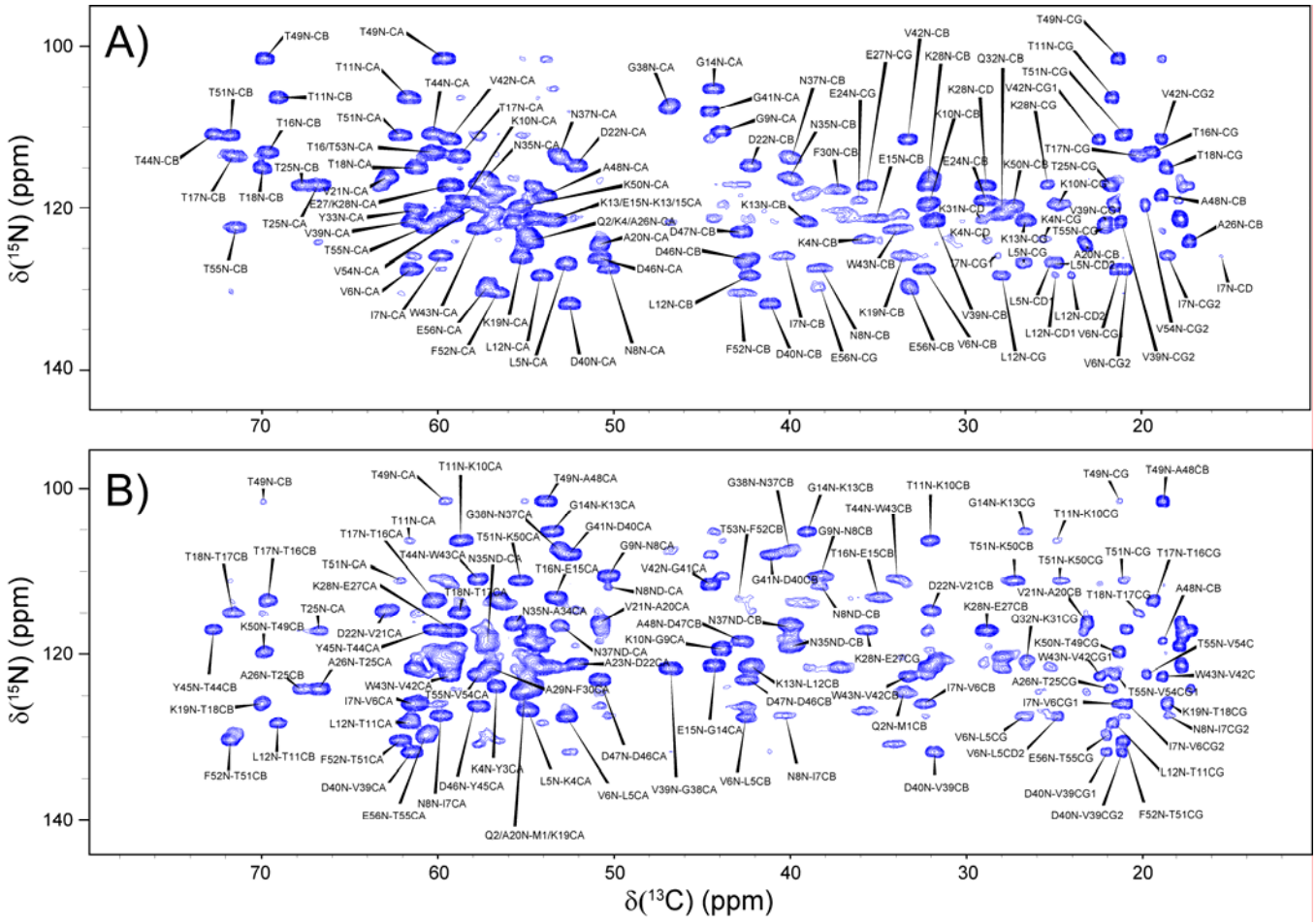


**Figure S2.** Regions from (A) 2D N(CA)CX and (B) N(CO)CX spectra for GB3 recorded at 500 MHz $^{1}$H frequency and 11.111 kHz MAS rate, indicating many of the assigned resonances. Spectra were recorded as 224* ($t_1$, $^{15}$N) × 1400* ($t_2$,$^{13}$C) data matrices with acquisition times of 20 ms ($t_1$) and 28 ms ($t_2$), and a measurement time of ~20 h per spectrum. Experimental parameters, N(CA)CX: $^{15}$N carrier at 120 ppm, $^{13}$C carrier at 80 ppm, 3.5 ms SPECIFIC CP with rf fields of ~7/2×$\omega_r$ on $^{15}$N and ~5/2×$\omega_r$ on $^{13}$C (tangent ramp), 15 ms $^{13}$C-$^{13}$C RAD/DARR mixing (Zilm, 1999; Takegoshi et al., 2001; Morcombe et al., 2004) (spectrum with 50 ms mixing was also recorded, data not shown); N(CO)CX: $^{15}$N carrier at 120 ppm, $^{13}$C carrier at 177 ppm, 6 ms SPECIFIC CP with rf fields of ~7/2×$\omega_r$ on $^{15}$N and ~5/2×$\omega_r$ on $^{13}$C (tangent ramp), 15 ms $^{13}$C-$^{13}$C RAD/DARR mixing (spectrum with 50 ms mixing was also recorded, data not shown); common parameters: 1 ms $^{1}$H-$^{15}$N CP (50 kHz $^{1}$H, ~40 kHz $^{15}$N with tangent ramp), 70 kHz TPPM $^{1}$H decoupling during $t_1$ and $t_2$, single $^{13}$C π-pulse centered in $t_1$ for $^{15}$N-$^{13}$C$^{\alpha}$/$^{13}$C′ J-decoupling. Cross-peaks are drawn with the lowest contour at ca. 10 times the rms noise level.

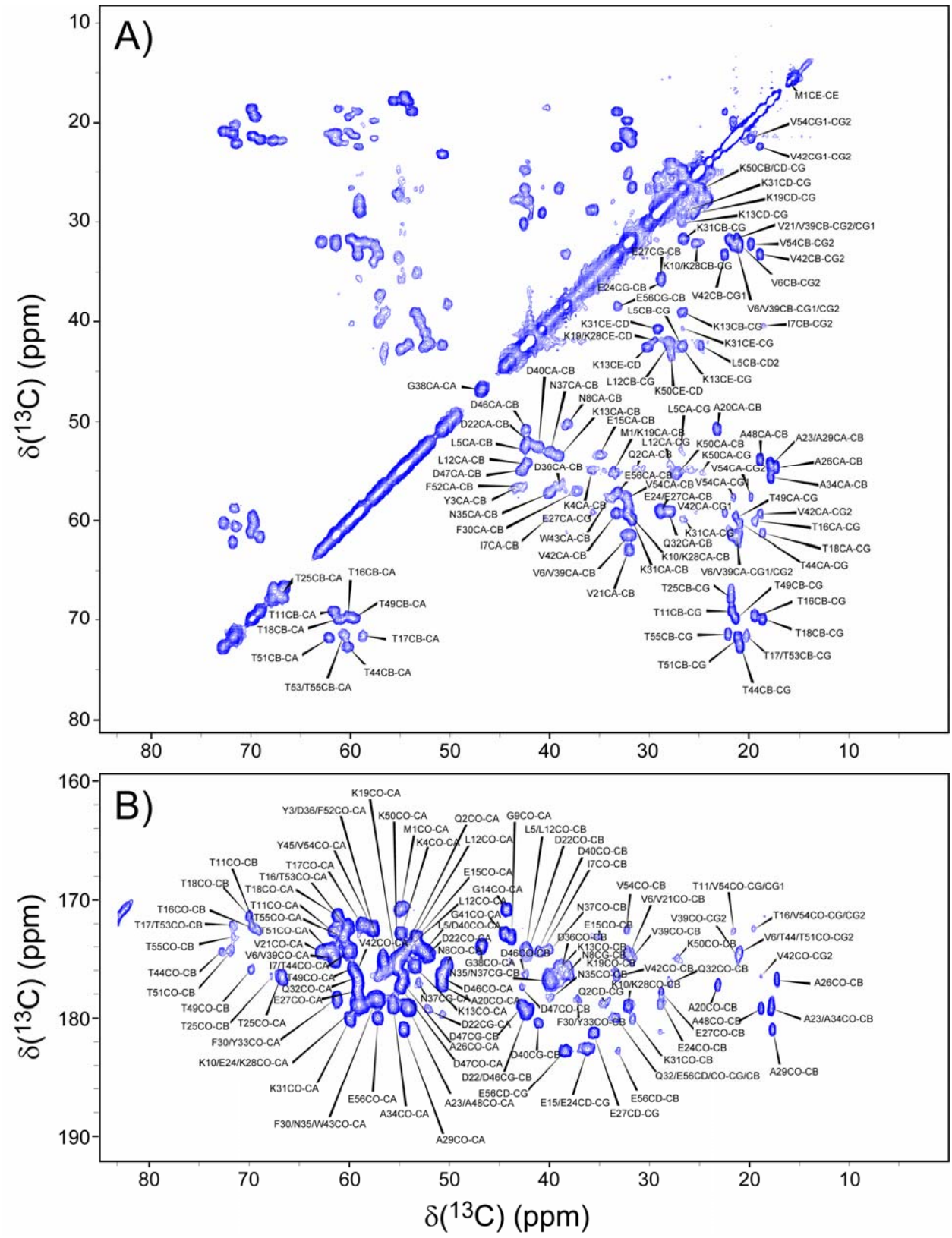


**Figure S3.** Regions from a 2D $^{13}C$-$^{13}C$ spectrum showing the $^{13}C^{aliphatic}$-$^{13}C^{aliphatic}$ (A) and $^{13}C'$-$^{13}C^{aliphatic}$ (B) correlations. Data were acquired at 500 MHz $^{1}H$ frequency and 11.111 kHz MAS using the RAD/DARR pulse scheme with a 5 ms mixing time (a spectrum with a 25 ms mixing time was also recorded, data not shown), and 70 kHz TPPM $^{1}H$ decoupling during $t_1$ and $t_2$. The spectrum was recorded as a 1024 ($t_1$, $^{13}C$) × 1400* ($t_2$,$^{13}C$) data matrix with acquisition times of 15.4 ms ($t_1$) and 28 ms ($t_2$), and a measurement time of 11 h. Cross-peaks are drawn with the lowest contour at ca. 10 times the rms noise level.

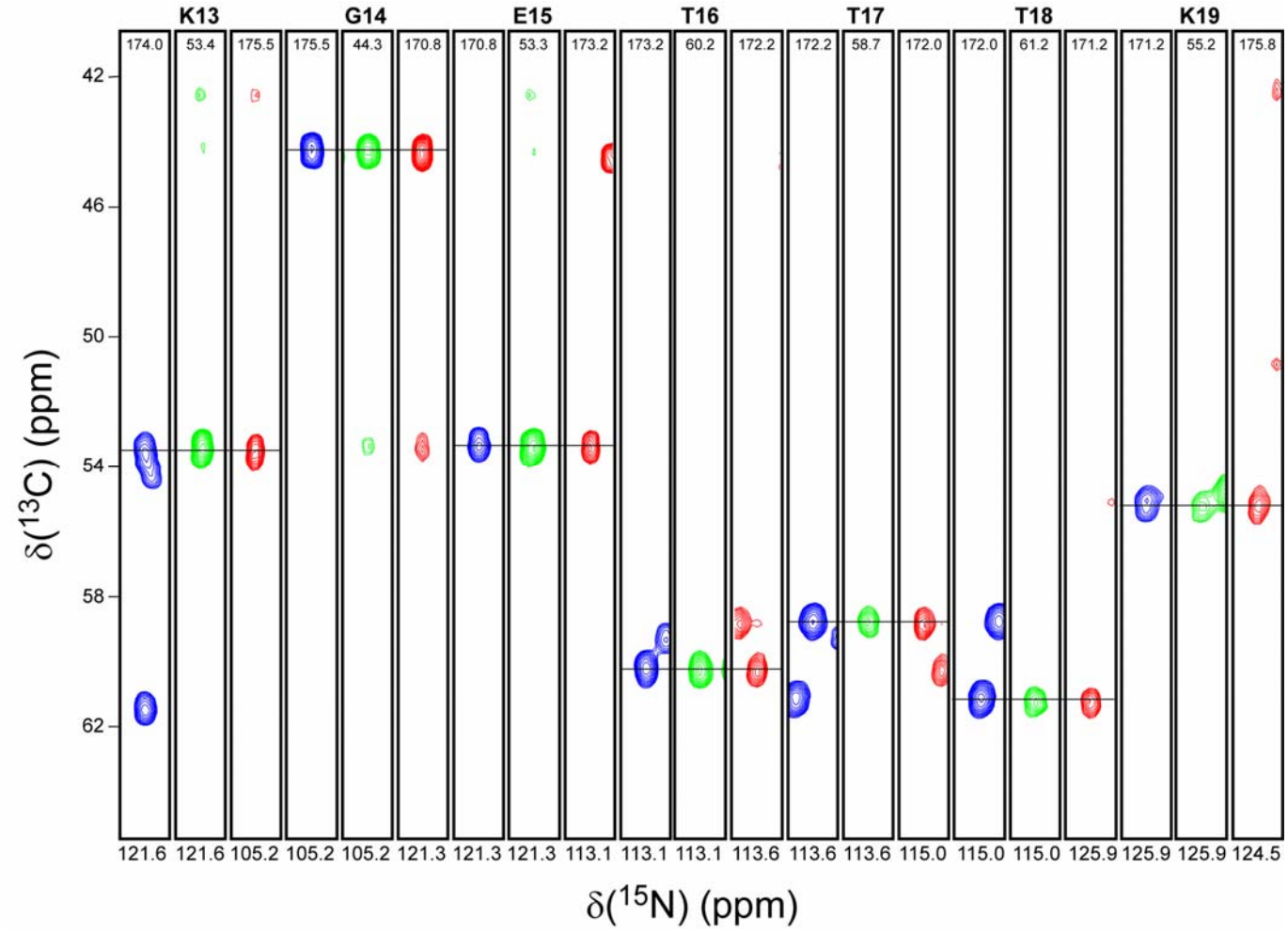


**Figure S4.** Representative [$F_1$($^{15}$N), $F_3$($^{13}$C)]-strips from 3D CONCA (blue contours), NCACX (green contours) and NCOCX (red contours) spectra of GB3 recorded at 500 MHz $^{1}$H frequency and 11.111 kHz MAS rate. Small regions corresponding to the $C^{\alpha}$ frequency in $F_3$ are shown for residues K13-K19 in the β2-strand (residue numbers are indicated above the NCACX strips). For the $i^{th}$ residue, the $F_1$($^{15}$N) and $F_2$($^{13}$C) frequencies listed below and inside each strip, respectively, correspond to $N_i/C'_{i-1}$ (CONCA), $N_i/C^{\alpha}_i$ (NCACX) and $N_{i+1}/C'_i$ (NCOCX). Experimental parameters, CONCA: $^{15}$N carrier at 120 ppm, $^{13}$C carrier at 177 ppm, 1.2 ms $^{1}$H-$^{13}$C CP with linear ramp, 6 ms SPECIFIC N-CO CP, 10 ms SPECIFIC N-CA CP with phase modulation on $^{13}$C for an effective 56 ppm carrier frequency, rf fields of ~7/2×$\omega_r$ on $^{15}$N and ~5/2×$\omega_r$ on $^{13}$C for both CP steps with tangent ramps on $^{13}$C, 32* ($t_1$, $^{15}$N) × 16* ($t_2$,$^{13}$C) × 1400* ($t_3$,$^{13}$C) data matrix with acquisition times of 11.2 ms ($t_1$), 5.4 ms ($t_2$) and 28 ms ($t_3$), total measurement time 6 h; NCACX: $^{15}$N carrier at 120 ppm, $^{13}$C carrier at 56 ppm, 1.2 ms $^{1}$H-$^{15}$N CP with linear ramp, 3.5 ms SPECIFIC N-CA CP with rf fields of ~5/2×$\omega_r$ on $^{15}$N and ~3/2×$\omega_r$ on $^{13}$C (tangent ramp), 50 ms $^{13}$C-$^{13}$C DARR mixing, 64* ($t_1$, $^{15}$N) × 64* ($t_2$,$^{13}$C) × 1400* ($t_3$,$^{13}$C) data matrix with acquisition times of 11.3 ms ($t_1$), 11.3 ms ($t_2$) and 28 ms ($t_3$), total measurement time 45 h; NCOCX: $^{15}$N carrier at 120 ppm, $^{13}$C carrier at 177 ppm, 1.2 ms $^{1}$H-$^{15}$N CP with linear ramp, 6 ms SPECIFIC N-CO CP with rf fields of ~7/2×$\omega_r$ on $^{15}$N and ~5/2×$\omega_r$ on $^{13}$C (tangent ramp), 50 ms DARR mixing, 80* ($t_1$, $^{15}$N) × 48* ($t_2$,$^{13}$C) × 1400* ($t_3$,$^{13}$C) data matrix with acquisition times of 14.2 ms ($t_1$), 8.5 ms ($t_2$) and 28 ms ($t_3$), total measurement time 42 h. In each spectrum the cross-peaks are drawn with the lowest contour at ca. 15 times the rms noise level.

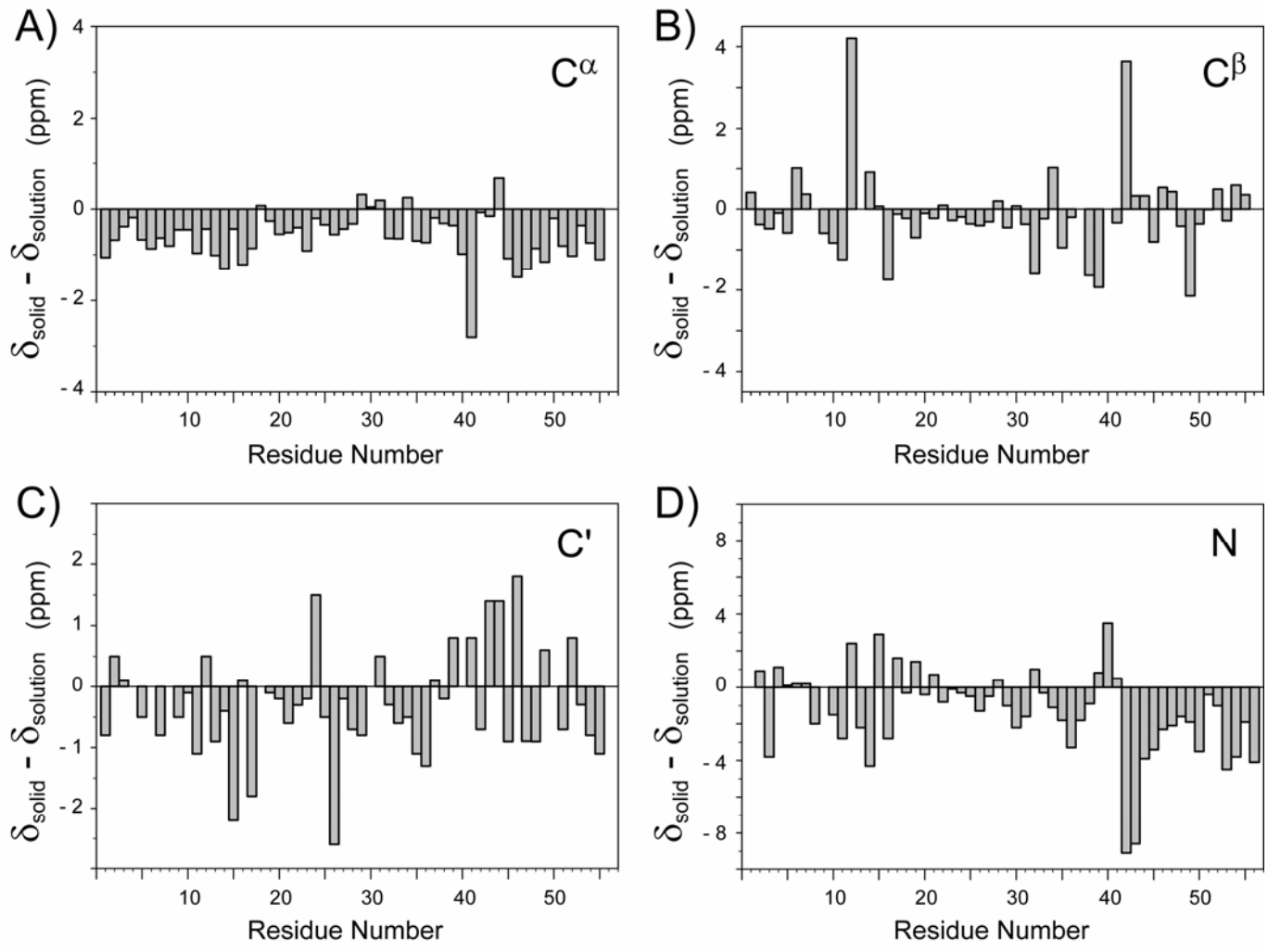


**Figure S5.** Comparison of (A) $^{13}C^{\alpha}$, (B) $^{13}C^{\beta}$, (C) $^{13}C'$, and (D) $^{15}N$ chemical shifts for GB3 in solution and solid-state. The mean differences ($\delta_{solid} - \delta_{solution}$) are, $^{13}C^{\alpha}$: -0.6 ± 0.5 ppm; $^{13}C^{\beta}$: -0.1 ± 1.1 ppm; $^{13}C'$: -0.3 ± 0.8 ppm; $^{15}N$: -1.3 ± 2.4 ppm. The magnitude of the observed chemical shift differences is similar to those observed for microcrystalline GB1 (Franks et al., 2005).

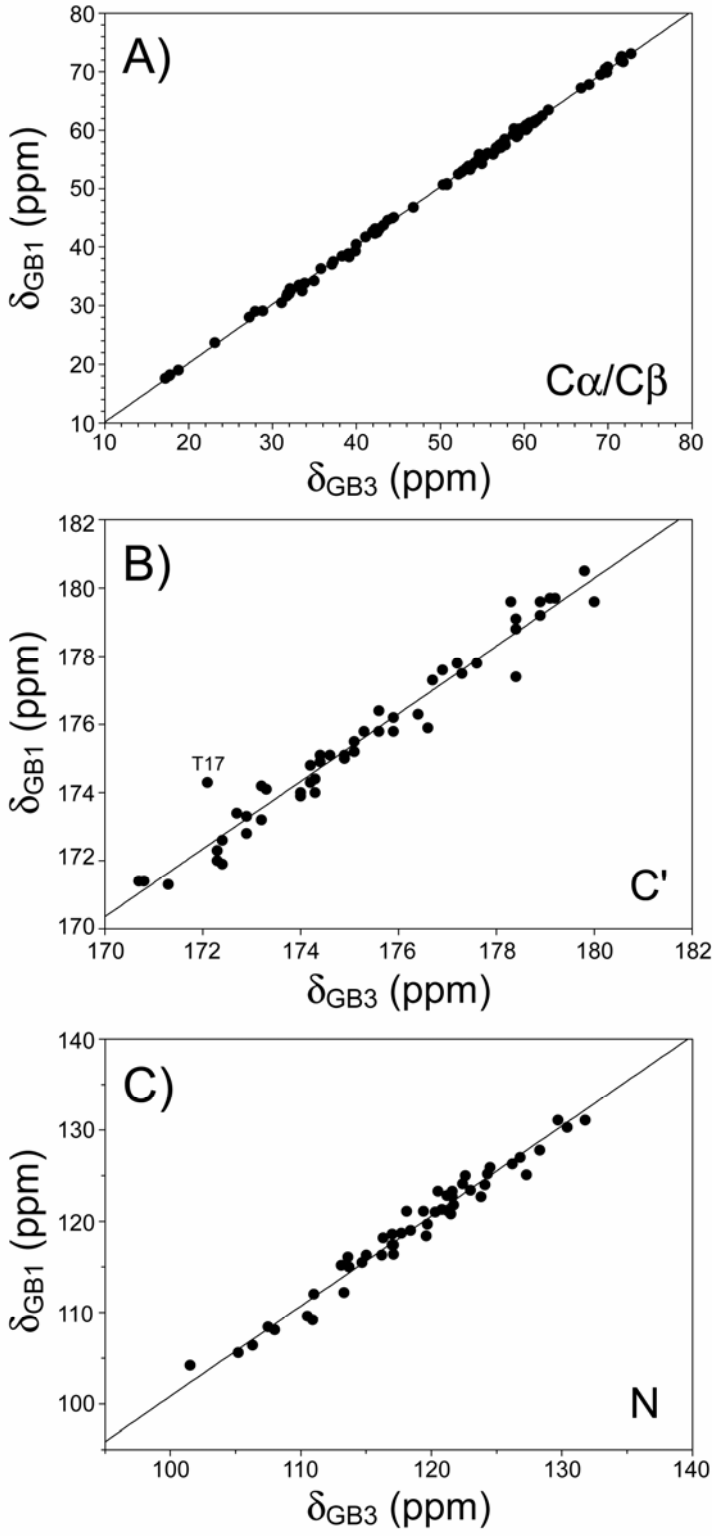


**Figure S6.** Comparison of (A) $^{13}C^{\alpha}/^{13}C^{\beta}$, (B) $^{13}C'$, and (C) $^{15}N$ chemical shifts for GB3 and GB1 (Franks et al., 2005) in the microcrystalline solid phase. Residues where GB1 and GB3 differ (6, 7, 19, 24, 29, 42) were excluded. The best-fit lines shown in the graphs, obtained by using regression analysis are: (A) $\delta_{GB1} = (1.003 \pm 0.003)\delta_{GB3} + (0.12 \pm 0.17)$, $R^2 = 0.999$; (B) $\delta_{GB1} = (0.993 \pm 0.029)\delta_{GB3} + (2 \pm 5)$, $R^2 = 0.959$; (C) $\delta_{GB1} = (0.988 \pm 0.013)\delta_{GB3} + (2.0 \pm 1.5)$, $R^2 = 0.992$, indicating that, as in solution, GB1 and GB3 likely adopt a very similar fold in the microcrystalline phase. The mean chemical shift differences ($\delta_{GB3} - \delta_{GB1}$) are, $^{13}C^{\alpha}$: -0.3 ± 0.4 ppm; $^{13}C^{\beta}$: -0.2 ± 0.5 ppm; $^{13}C'$: -0.2 ± 0.6 ppm; $^{15}N$: -0.6 ± 1.2 ppm. For the GB1 and GB3 chemical shifts included in the comparison, 143 out of 150 $^{13}C$ shifts are within 1 ppm (the only shift with a deviation >2 ppm was T17 CO, $|\Delta\delta| = 2.2$ ppm), and 43 out of 50 $^{15}N$ shifts are within 2 ppm (the largest deviation was 3.0 ppm for D36).

**References**


Baldus M, Petkova AT, Herzfeld J and Griffin RG (1998), "Cross polarization in the tilted frame: assignment and spectral simplification in heteronuclear spin systems", *Mol. Phys.*, **95**, 1197-1207.

Bennett AE, Rienstra CM, Auger M, Lakshmi KV and Griffin RG (1995), "Heteronuclear decoupling in rotating solids", *J. Chem. Phys.*, **103**, 6951-6957.

Delaglio F, Grzesiek S, Vuister GW, Zhu G, Pfeifer J and Bax A (1995), "NMRPipe: a multidimensional spectral processing system based on UNIX pipes", *J. Biomol. NMR*, **6**, 277-293.

Franks WT, Zhou DH, Wylie BJ, Money BG, Graesser DT, Frericks HL, Sahota G and Rienstra CM (2005), "Magic-angle spinning solid-state NMR spectroscopy of the β1 immunoglobulin binding domain of protein G (GB1): $^{15}$N and $^{13}$C chemical shift assignments and conformational analysis", *J. Am. Chem. Soc.*, **127**, 12291-12305.

Goddard TD and Kneller DG "SPARKY 3", University of California, San Francisco.

Gullion T, Baker DB and Conradi MS (1990), "New, compensated Carr-Purcell sequences", *J. Magn. Reson.*, **89**, 479-484.

Hediger S, Meier BH and Ernst RR (1995), "Adiabatic passage Hartmann-Hahn cross-polarization in NMR under magic-angle sample spinning", *Chem. Phys. Lett.*, **240**, 449-456.

Marcombe CR and Zilm KW (2003), "Chemical shift referencing in MAS solid state NMR", *J. Magn. Reson.*, **162**, 479-486.

Morcombe CR, Gaponenko V, Byrd RA and Zilm KW (2004), "Diluting abundant spins by isotope edited radio frequency field assisted diffusion", *J. Am. Chem. Soc.*, **126**, 7196-7197.

Takegoshi K, Nakamura S and Terao T (2001), "$^{13}$C-$^{1}$H dipolar-assisted rotational resonance in magic-angle spinning NMR", *Chem. Phys. Lett.*, **344**, 631-637.

Zilm KW (1999) in *40th Experimental NMR Conference*, Orlando, FL.